ARTICLE   **Open Access**

Spontaneous Small Biskyrmions in a Centrosymmetric Rare-Earth Kagome Ferrimagnet

Shulan Zuo [1], Kaiming Qiao[2], Zhan Wang[3], Ying Zhang [3,4], Chengbao Jiang [1] and Baogen Shen [3,5]

Abstract

Magnetic skyrmions with nontrivial topologies have great potential to serve as memory cells in novel spintronic devices. Small skyrmions were theoretically and experimentally confirmed to be generated under the influence of external fields in ferrimagnetic films via Dzyaloshinskii–Moriya interactions (DMIs). However, this topological state has yet to be verified in ferrimagnetic crystals, especially in the absence of external fields and DMIs. Here, spontaneous biskyrmions were directly observed in the $Tb_{0.2}Gd_{0.8}Co_2$ ferrimagnetic crystal with a Kagome lattice using Lorentz transmission electron microscopy. The high-density biskyrmions exhibited a small size (approximately 50 nm) over a wide temperature range, were closely related to subtle magnetic interaction competition, and coexisted with some broken stripes that could be easily converted into zero-field biskyrmions by utilizing proper field-cooling manipulation. These results can be used to establish a platform for investigating functional sub-50-nm skyrmions in ferrimagnetic crystals and to facilitate advanced applications in magnetic devices.

Introduction

Topologically protected magnetic skyrmions are promising candidates for serving as memory bits in future spintronic devices. This unique magnetic texture was initially studied in bulk chiral magnets via Dzyaloshinskii–Moriya interactions (DMIs)[1,2], followed by magnetic multilayers with interfacial DMIs[3,4]. In addition to chiral materials, skyrmions can also be stabilized by the competition between dipolar interactions and uniaxial magnetic anisotropy in centrosymmetric materials without DMI[5,6]. In recent decades, magnetic skyrmions have been intensively studied in ferromagnetic materials with[7–9] or without[10–12] DMIs, including their dynamic behavior under external fields[5,9,13]. To achieve their potential applications, topological spin textures with small sizes (tens of nanometers in diameter) and ease of manipulation are highly pursued[14–16]. However, the bit size is restricted

in ferromagnetic skyrmions because of the large stray field interaction in ferromagnetic materials[15,16].

Theoretically, this limitation can be best addressed for antiferromagnetically exchange-coupled skyrmions because of the presence of two equivalent and antiparallel magnetic sublattices[17,18]; thus, the skyrmions in antiferromagnets are predicted to be small in size and exhibit better current-driven behavior. However, the manipulation and observation of spin textures in antiferromagnetic materials are technically difficult to achieve[19]. Recently, skyrmions in ferrimagnetic films were observed and found to have the advantages of antiferromagnetic skyrmions due to their same antiparallelly aligned magnetic sublattices[14,20]. Despite recent progress, ferrimagnetic (anti) skyrmions have been observed in very few materials, where an external force such as an external magnetic field is typically required for the nucleation of skyrmions[14,20–26], and the size of skyrmions critically depends on the DMI[20,21,27,28]. Therefore, it remains an open question whether small skyrmions can be stabilized in ferrimagnetic materials without the DMI. Moreover, the requirement of external fields for skyrmion nucleation causes a more complex device design because additional

Correspondence: Shulan Zuo (zuoshulan@buaa.edu.cn) or
Kaiming Qiao (kmqiao@ustb.edu.cn) or Ying Zhang (zhangy@iphy.ac.cn)
[1]School of Materials Science and Engineering, Beihang University, Beijing, PR China
[2]School of Materials Science and Engineering, University of Science and Technology Beijing, Beijing, PR China
Full list of author information is available at the end of the article

fields are needed to produce them. Considering the well-documented spontaneous skyrmions without the need for any external fields[29–33] and metastable skyrmions[34,35] in ferromagnetic materials, spontaneous small skyrmions and their manipulation are highly desirable in ferrimagnetic materials to advance their specialty.

Here, we directly observed spontaneous biskyrmions in the centrosymmetric ferrimagnetic crystal $Tb_{0.2}Gd_{0.8}Co_2$ utilizing Lorentz transmission electron microscopy (LTEM). The ferrimagnetic $Tb_xGd_{1-x}Co_2$ complex with frustrated Co Kagome lattices[36] involves a morphotropic phase boundary (MPB)[37], and its magnetic anisotropy can be easily tuned by controlling the rare-earth elements because the heavy rare earth element Tb has a much larger magnetocrystalline anisotropy than Gd. Thus, we achieve substantial control over magnetic interactions governing topological states, and the generation mechanism of spontaneous biskyrmions has been revealed by combining micromagnetic simulations. In contrast to the biskyrmions in ferromagnetic materials with a typical size close to or much larger than 100 nm[5,7], spontaneous biskyrmions in $Tb_{0.2}Gd_{0.8}Co_2$ exhibit a stable size of approximately 50 nm over a wide temperature range. Moreover, simple field cooling (FC) manipulation can easily transform the coexisting stripes into zero-field biskyrmions, which may benefit from the easily changing magnetization configuration under a small external magnetic field near the MPB. Our findings could stimulate additional research on skyrmions in ferrimagnetic crystals with potential application in skyrmion-based spintronic devices.

Materials and methods

$Tb_xGd_{1-x}Co_2$ ($x = 0$, 0.2, 0.5) alloys with nominal components were prepared by arc melting in an argon atmosphere, and high-purity (99.9%) elements of Tb, Gd, and Co were used. Additional rare-earth elements (3%) above the stoichiometric composition were added to compensate for the weight loss during arc melting. The as-prepared ingots were sealed in a quartz tube under a high-purity argon atmosphere, annealed at 1373 K for 24 h, and then quenched in liquid nitrogen to ensure homogeneity. The crystal structure of the sample was characterized using powder X-ray diffraction (XRD) (Rigaku SmartLab diffractometer with Cu K_α radiation).

The basic magnetic properties of the sample were measured using a superconducting quantum interference device–vibrating sample magnetometer (SQUID–VSM). An oriented polycrystalline sample was prepared by aligning milled powders with epoxy resin under a field of 3 T at room temperature to calculate magnetic anisotropy constants using the Sucksmith–Thompson method[38].

A polycrystalline bulk sample was cut into slices that were thinned by mechanical polishing, dimpling, and argon ion milling to prepare the sample for LTEM observation. The thickness of the LTEM sample was measured to be

approximately 108 nm by using the electron energy loss spectrum obtained via TEM (Fig. S1). The Fresnel LTEM method was employed in a JEOL-dedicated LTEM (JEOL 2100 F) with a negligible remnant magnetic field around the sample to observe magnetic domain structures. In this method, magnetic domain walls could be imaged as bright or dark contrast on defocused (under- or overfocus) image planes because of the deflected electron beam caused by the Lorentz force. The temperature dependence of the magnetic domain evolution was studied using a liquid-nitrogen TEM sample holder with a nominal temperature range of 120–300 K. Defocus values ranging from 400 to 700 μm were used. A small perpendicular magnetic field was applied during the FC manipulation by gradually increasing the objective lens current. Magnetic field-dependent magnetic field evolution was observed via conventional TEM (JEOL 2100 F) under a Fresnel model, where a perpendicular magnetic field was applied by gradually increasing the objective lens current. The detailed magnetization distribution was obtained by analyzing defocused LTEM images using commercial QPt software that is based on the transport-of-intensity equation (TIE)[39]. In the final images obtained by the TIE analysis, the colors and arrows depict the magnitude and direction of the magnetization distribution, respectively, while the dark color represents the out-of-plane magnetization.

Micromagnetic simulations were performed by using a 3D object-oriented micromagnetic framework (OOMMF) code based on the Landau–Lifshitz–Gilbert equation[40]. A thin plate of $1000 \times 1000 \times 100$ nm^3 modeled by a rectangular mesh of $4 \times 4 \times 4$ nm^3 was used under periodic boundary conditions to study the magnetic texture changes with the key magnetic parameters (*i.e.*, M_s and K_u). The ferrimagnetic alloy was simplified into a ferromagnetic system while performing micromagnetic simulations. An initial configuration with randomly distributed magnetization was used in calculating the phase diagram, and a spontaneous biskyrmion configuration was employed as the initial state to study the biskyrmion evolution with temperature using experimental parameters at zero fields. The exchange constant A was estimated to be $A = 3.4 \times 10^{-11}$ J/m using $\delta = 2\sqrt{A/K_u}$, where the domain wall width δ was measured to be approximately 22.6 nm from the LTEM images at room temperature. The skyrmion number of a simulated biskyrmion was integrated in the x- and y-directions using $N_{sk} = \frac{1}{4\pi} \iint \boldsymbol{n} \cdot (\frac{\partial \boldsymbol{n}}{\partial x} \times \frac{\partial \boldsymbol{n}}{\partial y}) dx dy$, where $\boldsymbol{n}$ denotes the direction vector of magnetization[13].

Results and discussion
Observation of spontaneous small biskyrmions over a broad temperature range

The ferrimagnetic $Tb_xGd_{1-x}Co_2$ system features an MPB in which the easy magnetization direction and
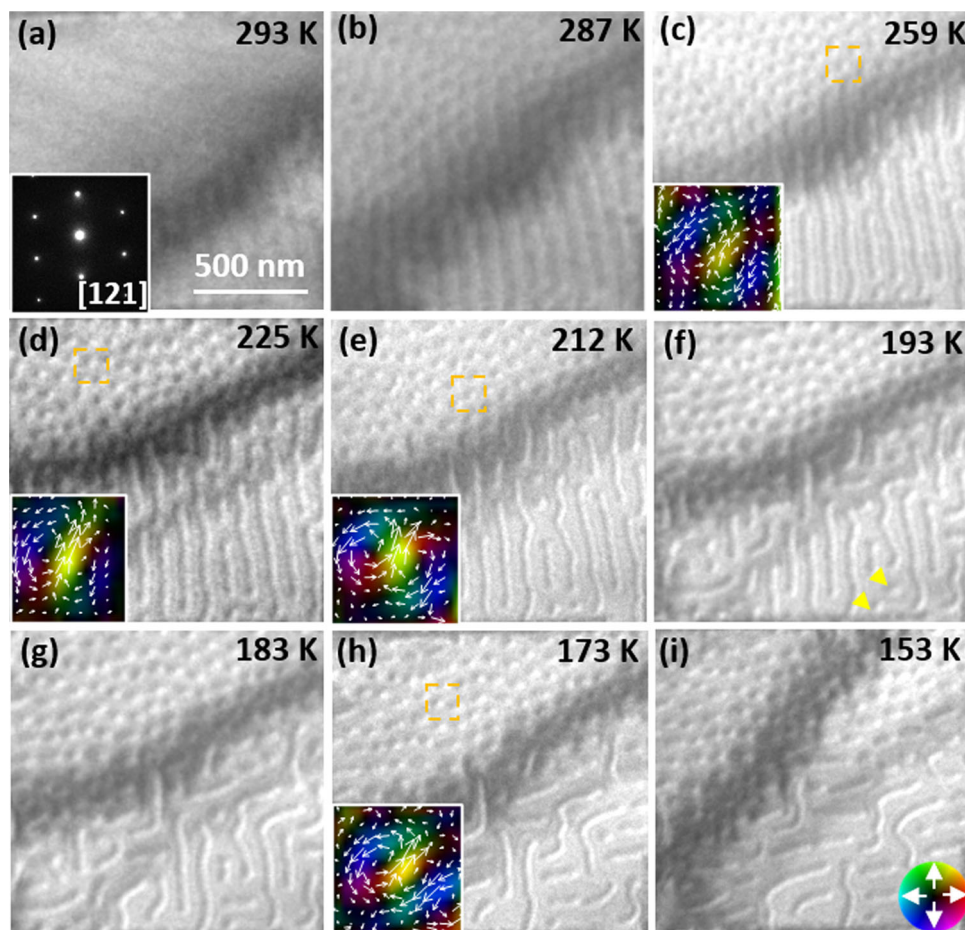
Fig. 1 Spontaneous biskyrmions in the ferrimagnetic crystal Tb$_{0.2}$Gd$_{0.8}$Co$_2$ at zero field. a Under-focused LTEM image of weak stripe domains at room temperature. The inset shows the selected area electron diffraction along the [121] zone axis. **b** Biskyrmions spontaneously arise at which there are no stripes. **c** The magnetic contrast of the biskyrmions becomes clearer. The inset shows the spin configuration of the selected biskyrmion obtained by transport-of-intensity equation (TIE) analysis. **d–i** Spontaneous biskyrmions remain robust with increasing temperature, while stripes evolve with temperature due to the gradually changing magnetic anisotropy. The insets in **d, e, h** show the spin configurations of single biskyrmions at different temperatures. The inset in **i** shows the color wheel depicting the magnetization magnitude and direction of the in-plane magnetic induction component, where the dark color denotes the out-of-plane magnetization.

crystal structure change simultaneously as the rare-earth element composition is varied, resulting in abundant physical properties[37]. The crystalline material with a TbCo$_2$-rich composition is a rhombohedral structure with an easily magnetized [111] axis below the Curie temperature (T_C), and the material with a GdCo$_2$-rich composition is tetragonal with an easily magnetized [001] axis[41,42]. The polycrystal Tb$_x$Gd$_{1-x}$Co$_2$ ($x = 0$, 0.2, 0.5) was prepared with different Tb-to-Gd ratios to tune its intrinsic magnetic properties (Fig. S2a, b); here, the Curie temperature (T_C) decreased with increasing Tb concentration (Fig. S2a) and could be adjusted to higher than room temperature for convenient application. Our target compound, Tb$_{0.2}$Gd$_{0.8}$Co$_2$, with a Co Kagome lattice crystalized in a centrosymmetric rhombohedral structure (space group $R\bar{3}m$) below the T_C (Fig. S2c, d) with lattice
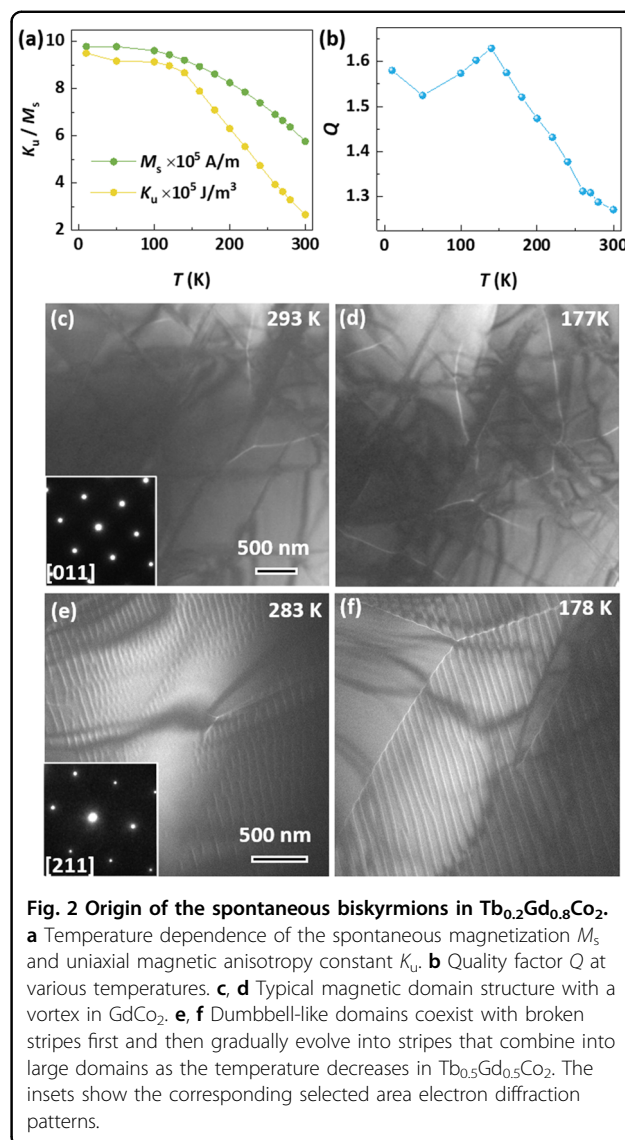
parameters a = b = 5.124(8) Å and c = 12.549(9) Å at room temperature and was a ferrimagnet with a Curie temperature of ~359 K (Fig. S2a).

Real-space observation of magnetic domain structures in Tb$_{0.2}$Gd$_{0.8}$Co$_2$ was performed using LTEM at various temperatures, as summarized in Fig. 1. At room temperature (293 K), a weak helical stripe pattern was observed (Fig. 1a). Upon cooling the plate, high-density nanodomains spontaneously formed (Fig. 1b) and coexisted with previous stripe domains. These nanodomains with half-white and half-black magnetic contrast became clearer as the temperature further decreased (Fig. 1c) and were identified as biskyrmions[5] by a combination of their the spin configuration (inset of Fig. 1c) obtained by TIE analysis. The spontaneous biskyrmions had a typical size of approximately 50 nm, which was smaller than that of

reported biskyrmions (approximately 100 nm) in other centrosymmetric materials[5]. As the sample was cooled to 153 K, the spontaneous biskyrmions remained robust and maintained their size together with spin textures almost unchanged (Fig. 1d–i), in contrast with previously reported spontaneous biskyrmions in ferromagnetic $NdCo_5$[33] and Nd_2Co_{17}[43] due to the different material nature. Notably, spontaneous biskyrmions always coexisted with broken stripes. In contrast to the initial stable biskyrmions, these stripes evolved with temperature (Fig. 1e–i), and some were converted into biskyrmions only at proper temperatures (indicated by yellow arrows in Fig. 1f). As the plate is heated to room temperature, spontaneous biskyrmions and stripes almost reversibly evolved, with the exception that the broken stripes more easily transformed into biskyrmions (Fig. S3). Half-white and half-black magnetic contrasts of biskyrmions in $Tb_{0.2}Gd_{0.8}Co_2$ could be clearly observed under different defocus values (Fig. S4), distinct from the magnetic contrast of type II bubbles.
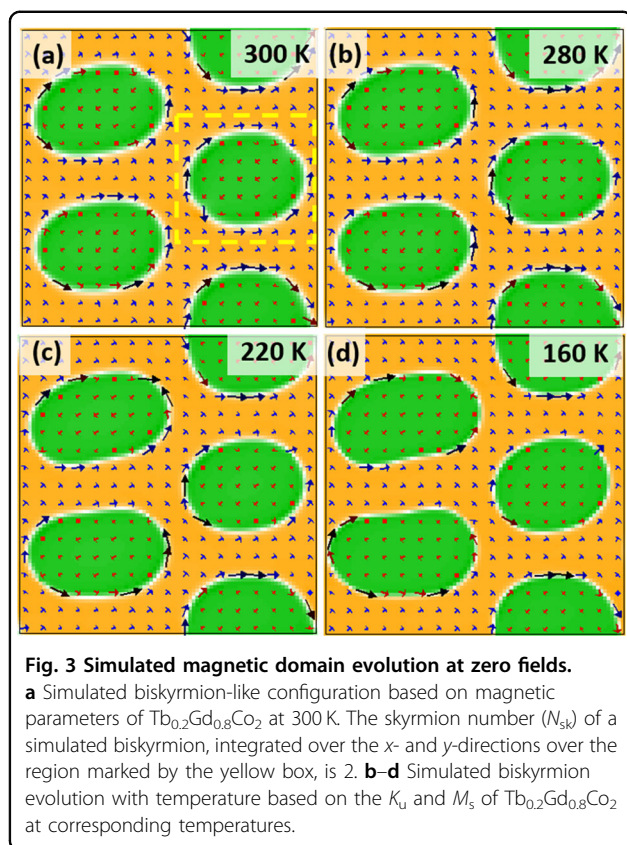
Physical origin of spontaneous biskyrmions

The competition between uniaxial magnetic anisotropy and dipolar interaction energies is a key factor in promoting skyrmions under external magnetic fields in previously reported centrosymmetric materials[5,44]. To determine the generation and stabilization mechanisms of small biskyrmions in $Tb_{0.2}Gd_{0.8}Co_2$, the temperature dependence of spontaneous magnetization (M_s) and the uniaxial magnetic anisotropy constant (K_u) (Fig. 2a) are derived from magnetization curves (Figs. S5 and S6; see Note 4 in the supplementary materials for more details). With decreasing temperature, M_s and K_u increase simultaneously. The quality factor Q, defined as the ratio of uniaxial magnetic anisotropy to stray field energy ($Q = K_u/K_d$), where $K_d = \mu_0 M_s^2/2$ and μ_0 is the vacuum permeability, was found to be between ~ 1.2 and ~ 1.7, as shown in Fig. 2b; this value is slightly greater than that for materials hosting skyrmions ($0 < Q < 1.0$) with the requirement of external fields[44]. Therefore, $Tb_{0.2}Gd_{0.8}Co_2$ is a soft magnet with relatively strong uniaxial anisotropy and weak dipolar interaction, that is, a combination of high K_u and low M_s; this is important for the formation of small skyrmions[14,16]. Q slightly increases as biskyrmions spontaneously form, indicating the key role of subtle competition between dipolar interactions and magnetic anisotropy in stabilizing skyrmions. Notably, the variation in Q is small over the entire temperature range (Fig. 2b), corresponding well with almost unchanged spontaneous biskyrmions with temperature once they form (Fig. 1). The dominant effects of M_s and K_u on promoting the stabilization of biskyrmions can be further confirmed by the observation of magnetic domain structures in $GdCo_2$ and $Tb_{0.5}Gd_{0.5}Co_2$. In the $Tb_xGd_{1-x}Co_2$ system, the

Fig. 2 Origin of the spontaneous biskyrmions in $Tb_{0.2}Gd_{0.8}Co_2$. **a** Temperature dependence of the spontaneous magnetization M_s and uniaxial magnetic anisotropy constant K_u. **b** Quality factor Q at various temperatures. **c, d** Typical magnetic domain structure with a vortex in $GdCo_2$. **e, f** Dumbbell-like domains coexist with broken stripes first and then gradually evolve into stripes that combine into large domains as the temperature decreases in $Tb_{0.5}Gd_{0.5}Co_2$. The insets show the corresponding selected area electron diffraction patterns.

spontaneous magnetization M_s decreases as the Tb concentration increases (Fig. 2a and Fig. S2b)[37]; this is contrary to the trend of magnetic anisotropy because Tb has greater magnetocrystalline anisotropy than Gd. Irregular large domains with magnetic vortexes (Fig. 2c,d and Fig. S7) are observed in $GdCo_2$ due to the low magnetic anisotropy related to Gd atoms; however, dumbbell-like domains emerge in $Tb_{0.5}Gd_{0.5}Co_2$ (Fig. 2e) because of enhanced magnetic anisotropy related to Tb atoms[37] and evolve into stripes (Fig. 2f) as the temperature decreases (see Fig. S8 for more information). Therefore, dipolar interactions and magnetic anisotropy work together to promote spontaneous biskyrmions, similar to previously reported biskyrmion materials[5] but requiring a slightly larger Q.

To better demonstrate the stabilization of spontaneous biskyrmions and their evolution in $Tb_{0.5}Gd_{0.5}Co_2$, micromagnetic simulations were performed based on the

Fig. 3 Simulated magnetic domain evolution at zero fields.
a Simulated biskyrmion-like configuration based on magnetic parameters of $Tb_{0.2}Gd_{0.8}Co_2$ at 300 K. The skyrmion number (N_{sk}) of a simulated biskyrmion, integrated over the x- and y-directions over the region marked by the yellow box, is 2. **b–d** Simulated biskyrmion evolution with temperature based on the K_u and M_s of $Tb_{0.2}Gd_{0.8}Co_2$ at corresponding temperatures.
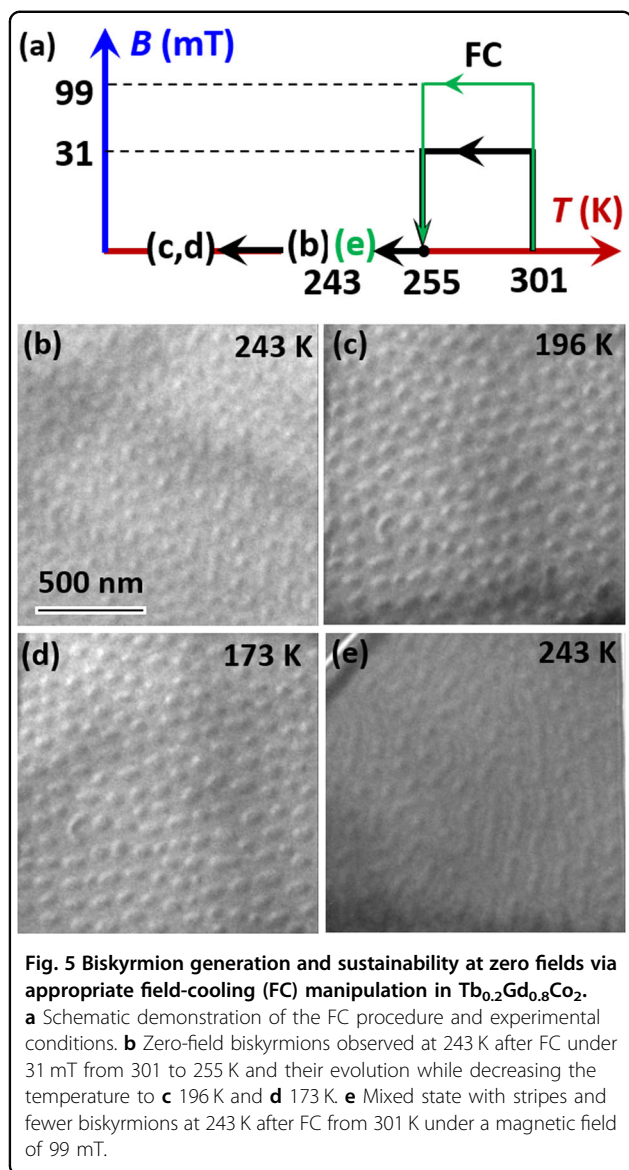
experimental results (Fig. 2a). Fig. S9 summarizes the simulated magnetic domain diagram as a function of the uniaxial magnetic anisotropy constant K_u and spontaneous magnetization M_s. The spontaneous nanodomains prefer to be present in certain combinations of K_u and M_s, which are marked using black dotted lines; this further shows the key role of the competition between the magnetic dipolar interaction and anisotropy energies. The experimental results of K_u and M_s for $Tb_{0.5}Gd_{0.5}Co_2$ are found to be within this combination range. The biskyrmion evolution with temperature was also simulated based on experimental parameters to illustrate the LTEM results (Fig. 1). The biskyrmion-like configuration can spontaneously form in the simulation based on the magnetic parameters at 300 K (Fig. 3a) and remains robust (Fig. 3b–d) as the magnetic parameters vary according to the experimental results at different temperatures (Fig. 2a); this result is similar to the magnetic domain evolution observed by LTEM (Fig. 1). Although there may be some differences in spin configurations obtained in the experiment and simulation, the micromagnetic simulation in Fig. 3a potentially shows the presence of the topological magnetic texture in this alloy.

Manipulation of biskyrmions in $Tb_{0.2}Gd_{0.8}Co_2$

In addition to the temperature-driven biskyrmion transition, the stripe domains could evolve into
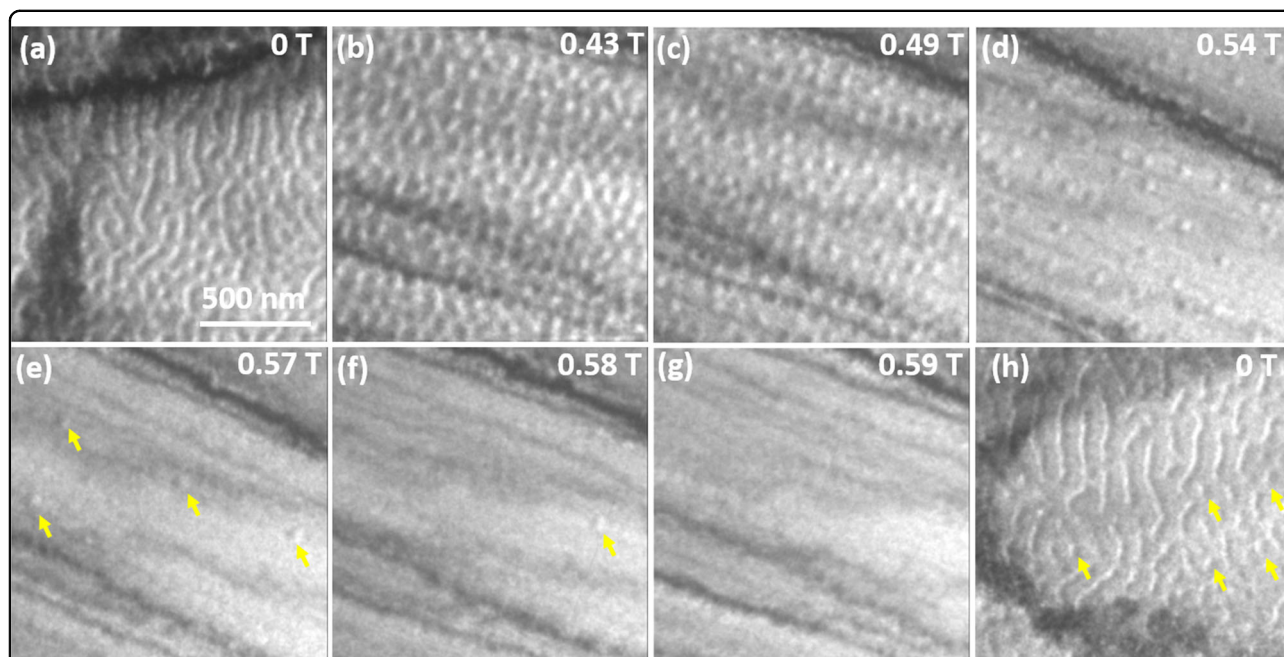
Fig. 4 Under-focused LTEM images of magnetic field-dependent biskyrmion evolution in $Tb_{0.2}Gd_{0.8}Co_2$ at 238 K. The magnetic field is applied perpendicularly to the thin plate. **a** Biskyrmions and stripe domains at zero field. **b** Stripe domains transform into biskyrmions as the magnetic field increases. **c, d** Biskyrmions gradually disappear, and then, **e, f** an isolated biskyrmion state forms with increasing magnetic field. **g** Saturated single domain state at a magnetic field of 0.59 T. **h** Biskyrmions coexist with the stripe domains at zero fields after removal of the magnetic field. The yellow arrows indicate the biskyrmions.

Fig. 5 Biskyrmion generation and sustainability at zero fields via appropriate field-cooling (FC) manipulation in Tb$_{0.2}$Gd$_{0.8}$Co$_2$. **a** Schematic demonstration of the FC procedure and experimental conditions. **b** Zero-field biskyrmions observed at 243 K after FC under 31 mT from 301 to 255 K and their evolution while decreasing the temperature to **c** 196 K and **d** 173 K. **e** Mixed state with stripes and fewer biskyrmions at 243 K after FC from 301 K under a magnetic field of 99 mT.

After an optimized FC manipulation ($B = 31$ mT), a biskyrmion state without stripes was obtained at zero field (Fig. 5b), in contrast to the mixed state of spontaneous biskyrmions and stripes in Fig. 1. The apparent magnetic field of 31 mT was smaller than that used in other reported materials[34], possibly benefiting from the characteristics of MPB[37]. These high-density zero-field biskyrmions (Fig. 5b) obtained by the FC process remained robust as the temperature changed (Fig. 5c,d), in contrast to the stripes in Fig. 1f−h. The fixed magnetic field in the FC procedure significantly influenced the biskyrmion density. The mixed state of stripes and biskyrmions (Fig. 5e) reappeared as the FC was performed at a higher magnetic field, which could cause agglomeration of the nucleation sites, thereby reducing the biskyrmion density[34]. The presence of tunable biskyrmions in the ferrimagnetic crystal Tb$_{0.2}$Gd$_{0.8}$Co$_2$ without the need for any external field or geometric constraints provided fundamental insight into the small skyrmions in ferrimagnetic crystals.

Conclusions

In summary, using LTEM, we directly observed the spontaneous emergence of small biskyrmions (approximately 50 nm) in the ferrimagnetic crystal Tb$_{0.2}$Gd$_{0.8}$Co$_2$ over a wide temperature range at zero fields. The attainment of these spontaneous biskyrmions was caused by the subtle tuning of the magnetic parameters utilizing rare-earth elements with different intrinsic properties to simultaneously achieve low M_s and larger K_u; these parameters are essential for achieving small skyrmions. The biskyrmions could be easily manipulated by employing a simple FC process, where the complete biskyrmion state was achieved after FC at a proper magnetic field and remained robust as the temperature changed. The presence of small spontaneous biskyrmions in Tb$_{0.2}$Gd$_{0.8}$Co$_2$ without the DMI, together with its tunable behavior under a small field, experimentally demonstrated an avenue for designing topological magnetic textures in ferrimagnetic materials. This discovery shed light on the exploitation of the spontaneous topological spin textures with small sizes in ferrimagnetic crystals and is highly important for achieving skyrmion-based spintronic devices.

Author details
[1]School of Materials Science and Engineering, Beihang University, Beijing, PR China. [2]School of Materials Science and Engineering, University of Science and

biskyrmions as the perpendicular magnetic field increases (Fig. 4a, b), while spontaneous biskyrmions remained robust under a small magnetic field. Under further increases in magnetic field strength, some biskyrmions annihilated (Fig. 4c, d), and the isolated biskyrmion state subsequently formed (Fig. 4e, f). As the magnetic field increased to 0.59 T, the biskyrmions disappeared and became a saturated single domain (Fig. 4g). The biskyrmion evolution was nearly reversible when the magnetic field was reduced from 0.59 to 0 T (Fig. S10), and some biskyrmions could remain stable even when the magnetic field was switched off (Fig. 4h).

Considering the tunable feature of magnetic configurations near the MPB, FC manipulation was performed by lowering the temperature at a constant perpendicular magnetic field B, as schematically depicted in Fig. 5a.

Technology Beijing, Beijing, PR China. ³Beijing National Laboratory for Condensed Matter Physics, Institute of Physics, Chinese Academy of Sciences, Beijing, PR China. ⁴Songshan Lake Materials Laboratory, Dongguan, Guangdong, China. ⁵Ningbo Institute of Materials Technology & Engineering, Chinese Academy of Sciences, Ningbo, Zhejiang, China

Author contributions

Conflict of interest

References

1. Mühlbauer, S. et al. Skyrmion lattice in a chiral magnet. *Science* **323**, 915–919 (2009).
2. Yu, X. Z. et al. Real-space observation of a two-dimensional skyrmion crystal. *Nature* **465**, 901–904 (2010).
3. Chen, G. et al. Tailoring the chirality of magnetic domain walls by interface engineering. *Nat. Commun.* **4**, 2671 (2013).
4. Jiang, W. et al. Skyrmions in magnetic multilayers. *Phys. Rep.* **704**, 1–49 (2017).
5. Yu, X. Z. et al. Biskyrmion states and their current-driven motion in a layered manganite. *Nat. Commun.* **5**, 3198 (2014).
6. Kurumaji, T. et al. Skyrmion lattice with a giant topological Hall effect in a frustrated triangular-lattice magnet. *Science* **365**, 914–918 (2019).
7. Takagi, R. et al. Low-field Bi-Skyrmion formation in a noncentrosymmetric chimney ladder ferromagnet. *Phys. Rev. Lett.* **120**, 037203 (2018).
8. Li, Y. et al. Topological Hall effect and magnetic states in the Nowotny chimney ladder compound $Cr_{11}Ge_{19}$. *Phys. Rev. B* **103**, 024445 (2021).
9. Schulz, T. et al. Emergent electrodynamics of skyrmions in a chiral magnet. *Nat. Phys.* **8**, 301–304 (2012).
10. Leonov, A. O. & Mostovoy, M. Multiply periodic states and isolated skyrmions in an anisotropic frustrated magnet. *Nat. Commun.* **6**, 8275 (2015).
11. Capic, D., Garanin, D. A. & Chudnovsky, E. M. Stabilty of biskyrmions in centrosymmetric magnetic films. *Phys. Rev. B* **100**, 014432 (2019).
12. Xiao, X. et al. Low-field formation of room-temperature biskyrmions in centrosymmetric MnPdGa magnet. *Appl. Phys. Lett.* **114**, 142404 (2019).
13. Nagaosa, N. & Tokura, Y. Topological properties and dynamics of magnetic skyrmions. *Nat. Nanotechnol.* **8**, 899–911 (2013).
14. Caretta, L. et al. Fast current-driven domain walls and small skyrmions in a compensated ferrimagnet. *Nat. Nanotechnol.* **13**, 1154–1160 (2018).
15. Jungwirth, T., Marti, X., Wadley, P. & Wunderlich, J. Antiferromagnetic spintronics. *Nat. Nanotechnol.* **11**, 231–241 (2016).
16. Buttner, F., Lemesh, I. & Beach, G. S. D. Theory of isolated magnetic skyrmions: from fundamentals to room temperature applications. *Sci. Rep.* **8**, 4464 (2018).
17. Barker, J. & Tretiakov, O. A. Static and dynamical properties of antiferromagnetic skyrmions in the presence of applied current and temperature. *Phys. Rev. Lett.* **116**, 147203 (2016).
18. Zhang, X., Zhou, Y. & Ezawa, M. Magnetic bilayer-skyrmions without skyrmion Hall effect. *Nat. Commun.* **7**, 10293 (2016).
19. Legrand, W. et al. Room-temperature stabilization of antiferromagnetic skyrmions in synthetic antiferromagnets. *Nat. Mater.* **19**, 34–42 (2020).
20. Woo, S. et al. Current-driven dynamics and inhibition of the skyrmion Hall effect of ferrimagnetic skyrmions in GdFeCo films. *Nat. Commun.* **9**, 959 (2018).
21. Wu, H. et al. Ferrimagnetic Skyrmions in topological insulator/ferrimagnet heterostructures. *Adv. Mater.* **32**, 2003380 (2020).
22. Nayak, A. K. et al. Magnetic antiskyrmions above room temperature in tetragonal Heusler materials. *Nature* **548**, 561–566 (2017).
23. Jena, J. et al. Elliptical Bloch skyrmion chiral twins in an antiskyrmion system. *Nat. Commun.* **11**, 1115 (2020).
24. Jena, J. et al. Observation of magnetic antiskyrmions in the low magnetization ferrimagnet $Mn_2Rh_{0.95}Ir_{0.05}Sn$. *Nano Lett.* **20**, 59–65 (2019).
25. Meshcheriakova, O. et al. Large noncollinearity and spin reorientation in the NovelMn2RhSnHeusler Magnet. *Phys. Rev. Lett.* **113**, 087203 (2014).
26. Sharma, A. K. et al. Nanoscale noncollinear spin textures in thin films of a D2d Heusler compound. *Adv. Mater.* **33**, e2101323 (2021).
27. Brandão, J., Dugato, D. A., Puydinger dos Santos, M. V., Béron, F. & Cezar, J. C. Tuning isolated zero-field skyrmions and spin spirals at room-temperature in synthetic ferrimagnetic multilayers. *Appl. Surf. Sci.* **585**, 152598 (2022).
28. Ma, C. T., Hartnett, T. Q., Zhou, W., Balachandran, P. V. & Poon, S. J. Tunable magnetic skyrmions in ferrimagnetic Mn_4N. *Appl. Phys. Lett.* **119**, 192406 (2021).
29. Rossler, U. K., Bogdanov, A. N. & Pfleiderer, C. Spontaneous skyrmion ground states in magnetic metals. *Nature* **442**, 797–801 (2006).
30. Ozawa, R., Hayami, S. & Motome, Y. Zero-field Skyrmions with a high topological number in itinerant magnets. *Phys. Rev. Lett.* **118**, 147205 (2017).
31. Hayami, S. & Motome, Y. Effect of magnetic anisotropy on skyrmions with a high topological number in itinerant magnets. *Phys. Rev. B* **99**, 094420 (2019).
32. Heinze, S. et al. Spontaneous atomic-scale magnetic skyrmion lattice in two dimensions. *Nat. Phys.* **7**, 713–718 (2011).
33. Zuo, S. et al. Spontaneous topological magnetic transitions in $NdCo_5$ rare-earth magnets. *Adv. Mater.* **33**, 2103751 (2021).
34. Peng, L. et al. Real-space observation of nonvolatile zero-field Biskyrmion lattice generation in MnNiGa magnet. *Nano Lett.* **17**, 7075–7079 (2017).
35. Karube, K. et al. Robust metastable skyrmions and their triangular-square lattice structural transition in a high-temperature chiral magnet. *Nat. Mater.* **15**, 1237–1242 (2016).
36. Huang, D. et al. Plateau-like magnetoresistance and topological Hall effect in Kagome magnets $TbCo_2$ and $DyCo_2$. *Appl. Phys. Lett.* **121**, 232404 (2022).
37. Zhou, C. et al. Inverse effect of morphotropic phase boundary on the magnetostriction of ferromagnetic $Tb_{1-x}Gd_xCo_2$. *Phys. Rev. B* **89**, 100101 (2014).
38. Sucksmith, W. & Thompson, J. E. The magnetic anisotropy of cobalt. *Proc. R. Soc. A* **225**, 362–375 (1954).
39. Ishizuka, K. & Allman, B. Phase measurement of atomic resolution image using transport of intensity equation. *J. Electron Microsc. (Tokyo)* **54**, 191–197 (2005).
40. Donahue, M. J. & Porter, D. G. OOMMF User's Guide, Interagency Report NISTIR Report No. NISTIR 6376 (NISTIR, 1999).
41. Gignoux, D., Givord, F. & Lemaire, R. Magnetic properties of single crystals of $GdCo_2$, $HoNi_2$, and $HoCo_2$. *Phys. Rev. B* **12**, 3878–3884 (1975).
42. Gignoux, D., Givord, F., de la Bathie Bathie, R. P. & Sayetat, F. Magnetic properties and spontaneous distortion in $TbCo_2$. *J. Phys. F: Met. Phys.* **9**, 763–772 (1979).
43. Zuo, S. et al. Spontaneous Biskyrmion lattice in a centrosymmetric rhombohedral rare-earth magnet with easy-plane anisotropy. *Nano Lett.* **23**, 550–557 (2023).
44. Montoya, S. A. et al. Tailoring magnetic energies to form dipole skyrmions and skyrmion lattices. *Phys. Rev. B* **95**, 024415 (2017).